This article has been accepted for publication in a future issue of this journal, but has not been fully edited. Content may change prior to final publication. Citation information: DOI 10.1109/JLT.2019.2952725, Journal of Lightwave Technology

The Impact of Local Oscillator Frequency Jitter and Laser Linewidth to Ultra High Baud Rate Coherent Systems

Rui Zhang, Wen-Jr Jiang, Konstantin Kuzmin, Yi Weng, Wenlong Mou, Gee-Kung Chang, *Fellow, IEEE, Fellow, OSA*, and Winston I. Way, *Fellow, IEEE, Fellow, OSA*

***Abstract*— Through theoretical analysis and simulation, we investigate the system impact due to a sinusoidal jitter tone and the resultant local oscillator (LO) laser linewidth requirement in ultra-high baud rate and long distance coherent optical systems. We also carried out experiments in 64Gbaud, dual-polarization (DP)-16QAM systems to verify the theoretical analysis and simulation. We have also obtained a jitter interference tolerance mask to qualify LO lasers. A jitter tone with a frequency lower than ~1MHz has a higher tolerance since it generally causes constant frequency or phase shift, which can be tracked by a receiver DSP. For a jitter tone with a frequency higher than ~1MHz, the tolerance becomes much tighter since the tone will affect laser lineshape and induce equalizer-enhanced phase noise (EEPN). Consequently, a jitter tone in the higher frequency region could severely affect the system performance. Theoretical analysis and numerical result illustrate that EVM^2 due to the effect of laser linewidth and a sinusoidal jitter tone is proportional to the weighted sum of $[\Delta\nu \times B_s \times L]$ and $[\Delta f_{pp} \times B_s \times L]^2$, where $\Delta\nu$ is the laser linewidth, B_s is the baud rate, Δf_{pp} is the laser peak-to-peak frequency deviation due to a sinusoidal jitter tone, and L is the fiber transmission length. This result is applicable for all orders of QAM constellations. The implication to future 100 Gbaud and beyond systems is delineated.**

***Index Terms*— Optical fiber communication, coherent communication, laser noise**

I. Introduction

With the explosive growth of data traffic from emerging bandwidth-consuming services such as the mission-critical Internet of Things (IoT), 4k/8k ultra-high definition video streaming, high-speed Internet, big data processing, and smartphones, coherent optical communication has become a mainstream solution to high data rate transmission [1, 2]. Tunable lasers are critical to optical networking and coherent optical transmission [3], and its linewidth is a key parameter which impacts system performance[4, 5]. Laser white frequency noise induces phase variation and EEPN for long-haul transmission. EEPN is from phase to amplitude noise conversion caused by intermixing of the received dispersed signal, and the phase-noise-induced sidebands of the local oscillator (LO) in a coherent system with post-reception electrical chromatic dispersion (CD) compensation [4, 6-8]. It was found that the EVM^2 due to EEPN is proportional to $[\Delta\nu \times B_s \times L)]$ [4]. However, the system performance impact due to sinusoidal interfering tones, which are caused by switching power supplies, power converters, and other circuit noise in pluggable modules and line-cards [9-13], have not been carefully studied.

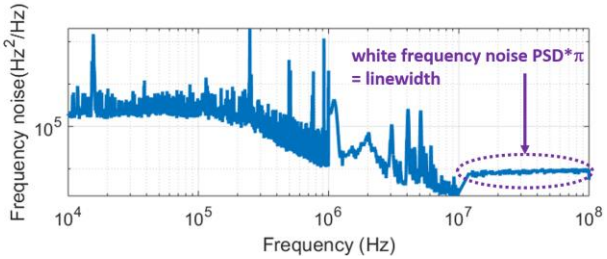

Fig 1. Measured laser frequency noise power spectral density (PSD) illustrating the existence of multiple interfering tones due to switching power supplies and circuit noise in a coherent pluggable module. Note that the interfering tones below 1MHz are found to be less damaging to the transmitted signal quality.

Figure 1 illustrates the frequency noise (FN) power spectral density (PSD), which can be measured from frequency to intensity fluctuation conversion by using a well-designed discriminator followed by intensity noise removing as shown in [14]. The FN PSD includes the white noise region above 10MHz (whose value multiplied by π is the laser linewidth [15]) and multiple interfering tones due to the switching power supplies and circuit noise in a pluggable coherent module. The white frequency noise region observed in the FN PSD is suitable for linewidth calculation in all kinds of lasers [15]. The frequency jitter tones have a peak-to-peak frequency deviation Δf_{pp} ranging between 0.1 MHz and several MHz. It is also worth noting that for future smaller pluggable coherent modules, switching power supplies would become more compact and consequently their switching frequencies (and therefore the induced jitter tone frequencies) would be increased beyond 1 MHz, which causes more degradations to the system performance (see Fig.5(d) in Sec.IV). Note that Δf_{pp} can be calculated from the power spectrum by carrying out $2\sqrt{2}sqrt(\cdot)$ operation on the power level of the sinusoidal interfering tone, which is the product of a tone amplitude in the frequency noise spectrum and its corresponding measurement resolution bandwidth. The impact of these interfering tones on high baud rate coherent systems is the main topic of our paper.

R. Zhang, and G.-K. Chang are with the School of Electrical and Computer Engineering, Georgia Institute of Technology, Atlanta, GA 30308 USA (e-mail: ruizhangece@gatech.edu; gkchang@ece.gatech.edu).

W.-J. Jiang, K. Kuzmin, Y. Weng, and W. I. Way are with NeoPhotonics, 3081 Zanker Road, San Jose, CA 95134, USA (e-mail: wen-jr.jiang@neophotonics.com; konstantin.kuzmin@neophotonics.com; yi.weng@neophotonics.com; winston.way@neophotonics.com).

W. Mou is with the department of Electrical Engineering and Computer Science, University of California at Berkeley, Berkeley, CA 94720 (e-mail: wmou@eecs.berkeley.edu).

This article has been accepted for publication in a future issue of this journal, but has not been fully edited. Content may change prior to final publication. Citation information: DOI 10.1109/JLT.2019.2952725, Journal of Lightwave Technology

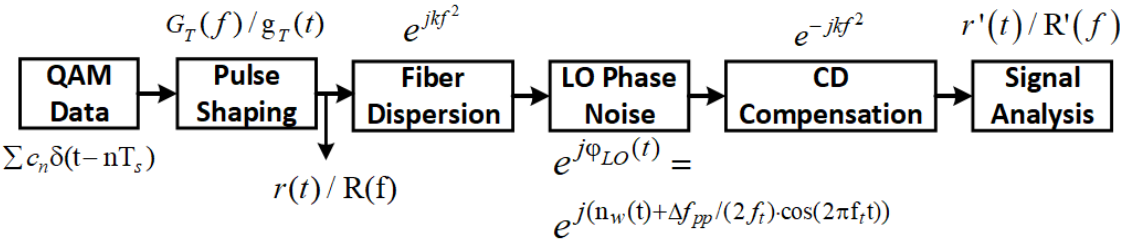

Fig 2. Block diagram of the theoretical analysis under the assumption of a perfect transmitter laser.

Through experiments, we obtained receiver jitter tolerance masks for 32 and 64 Gbaud DP-16QAM with a transmission distance up to 900km. We also performed a theoretical analysis of the EVM variation caused by jitter tone, which was verified by simulation and experiments. Note the result of theoretical analysis is also applicable to higher order modulation formats. We observed that the tone-induced phase to amplitude noise conversion through EEPN can cause a much tighter requirement on LO linewidth for higher baud rates (e.g., 100Gbaud), longer transmission distances (e.g., >600km), and higher order QAM (e.g., 16QAM or beyond).

The paper is organized as follows. In Section II, we present the theoretical analysis considering the jitter tone with a frequency higher than a corner frequency, where the corner frequency is dependent on the time duration of the carrier frequency offset (CFO) block. Section III depicts the experimental setup of the 32-Gbaud/64-Gbaud 16-QAM coherent systems. Section IV describes the simulation and experimental results, and Section V gives a concluding remark.

II. Theoretical Analysis

We perform a theoretical analysis using the block diagram shown in Fig.2. Assume that the symbol period is T_s, and c_n is the any order of QAM symbols in the complex data plane, the incoming QAM data train is modeled as $\sum c_n\delta(t-nT_s)$, which passes through an ideal Nyquist pulse shaping filter, whose interpolation function can be expressed as $g_T(t)=\mathrm{sinc}(t/T_s)$ to generate a band-limited signal. Considering the fact that EEPN mainly comes from a local oscillator (LO) rather than a transmitter in the post-CD compensation scheme [8], we assume a perfect transmitter laser and ignore the laser relative intensity noise (RIN). Based on the analysis in [4], after fiber dispersion, the time domain of the demodulated signal influenced by EEPN can be modeled as:

$$r'(t)=\int_{-\infty}^{\infty}X_{LO}(f_1)\cdot e^{-jkf_1^2}\cdot r(t-kf_1/\pi)e^{j2\pi f_1 t}\,df_1 \qquad (1)$$

where $X_{LO}(f_1)$ denotes the frequency response of the LO phase noise, which can be characterized as the Fourier transform of the phase fluctuation $e^{j\varphi_{LO}}$. In eq.(1), $k=\pi\cdot D\cdot L\cdot c\cdot f_c$ is the accumulated dispersion factor, where, D is the dispersion coefficient, c is light speed, f_c is the optical frequency. The transmitted signal after the Nyquist filter is $r(t)=\sum c_n\delta(t-nT_s)\otimes sinc(t/T_s)=\sum c_n sinc\left((t-nT_s)/T_s\right)$.

The theoretical analysis and numerical simulation in [4] have indicated that when only considering white frequency noise (laser linewidth), the square of error vector magnitude (EVM) is proportional to $\Delta\nu\times B_s\times L$. In our work, a more general model is established by incorporating not only the white frequency noise but also multiple sinusoidal jitter tones, i.e., the LO phase noise which be written as:

$$e^{j\varphi_{LO}}=\exp\left(j\left(\sum_t\Delta f_{pp_t}/(2f_t)\cdot\cos(2\pi f_t t+\varphi_t)+n_w(t)\right)\right) \qquad (2)$$

where Δf_{pp} and f_t are the peak-to-peak frequency deviation and the frequency of a sinusoidal jitter tone while φ_t corresponds to its initial phase, and $n_w(t)$ corresponds to the white frequency noise which is related to laser linewidth [16, 17].

A. LO phase noise power spectral density S(f)

We begin with deriving the general formula of a laser lineshape $S(f)$ when the laser phase noise is perturbed by a single sinusoidal jitter tone as a simplified case in eq (2). When considering only white frequency noise, $S(f)$ is modeled as a single Lorentzian distribution [4]. In the following analysis, we will show that when considering both white frequency noise and frequency jitter tone, $S(f)$ can be well approximated by a weighted combination of frequency-shifted Lorentzian distributions.

By using Bessel series expansion[18], we can obtain the spectrum of an LO phase noise with an interfering tone and white frequency noise as:

$$\begin{aligned}S(f)&=\mathbb{E}|X_{LO}(f)|^2\\&=\iint_{\mathbb{R}^2}\mathbb{E}\left(e^{j(n_w(t)-n_w(u))}\right)e^{2\pi j(t-u)f}\exp\left(j\frac{\Delta f_{pp}}{2f_t}(\cos(2\pi f_t t)-\cos(2\pi f_t u))\right)dtdu\\&=\iint_{\mathbb{R}^2}\mathbb{E}\left(e^{j(n_w(t)-n_w(u))}\right)e^{2\pi j(t-u)f}\left(\sum_{n=-\infty}^{\infty}J_n\left(\frac{\Delta f_{pp}}{2f_t}\right)e^{-2\pi jtnf_t}\right)\left(\sum_{n=-\infty}^{\infty}J_n\left(\frac{\Delta f_{pp}}{2f_t}\right)e^{2\pi junf_t}\right)dtdu.\end{aligned} \qquad (3)$$

where $J_n(z)=\sum_{m\ge0}\frac{(-1)^m}{(m+n)!}(z/2)^{2m+n}$ is the n-th order Bessel function.

The expectation involving Wiener process can reach a closed form formula by using the characteristic functions of Gaussian random variables [19]: $\mathbb{E}\left(e^{j(n_w(t)-n_w(u))}\right)=e^{-\pi\cdot\Delta\nu\cdot|t-u|}$.

For each term of the summation in Eq (3), by changing of variable ($r=t+u, z=t-u$), we have:

$$\begin{aligned}&\iint_{[0,T]^2}\mathbb{E}\left(e^{j(n_w(t)-n_w(u))}\right)e^{2\pi j(t-u)f}e^{-2\pi jtn_1 f_t}e^{-2\pi jun_2 f_t}dtdu\\&=\frac{1}{2}\int_{-T}^{T}e^{-\pi\cdot\Delta\nu\cdot|z|}e^{2\pi jzf}e^{-\pi jz(n_1+n_2)f_t}\int_{T-|z|}^{T+|z|}e^{-\pi jr(n_1-n_2)f_t}dr\,dz\\&\approx\begin{cases}\pi\int_{-T}^{T}e^{-\pi\cdot\Delta\nu\cdot|z|}e^{2\pi jz(f-nf_t)}dz, & n_1=n_2=n\\0, & n_1\neq n_2\end{cases}.\end{aligned} \qquad (4)$$

This article has been accepted for publication in a future issue of this journal, but has not been fully edited. Content may change prior to final publication. Citation information: DOI 10.1109/JLT.2019.2952725, Journal of Lightwave Technology

Therefore, we obtain:

$$\begin{aligned} S(\mathrm{f}) &\approx \pi \sum_{n=-\infty}^{\infty} J_n\left(\frac{\Delta f_{pp}}{2 f_t}\right)^2 \int_{-\infty}^{\infty} e^{-\pi \cdot \Delta \nu \cdot |z|} e^{2\pi j z(\mathrm{f}-\mathrm{nf}_t)} dz \\ &= \frac{1}{2} \sum_{n=-\infty}^{\infty} J_n\left(\frac{\Delta f_{pp}}{2 f_t}\right)^2 \frac{\Delta \nu}{(f-n f_t)^2+\Delta \nu^2} \\ &= \frac{1}{2} \sum_{n=-\infty}^{\infty} w_n S_l(f-n f_t) \end{aligned} \tag{5}$$

where $S_l(\cdot)$ is a Lorentzian-shaped function. Eq.(5) shows that the LO phase noise spectrum which includes an interfering tone and white frequency noise is given by a weighted average of frequency-shifted Lorentzian distributions, with the weight at a frequency nf_t given by $J_n\left(\frac{\Delta f_{pp}}{2 f_t}\right)^2$.

B. Derivation of EVM

The EVM caused by the phase to amplitude conversion in a receiver phase noise compensation block can be defined as the mean square error of the received signal after CD compensation normalized by the transmitted signal power [4]:

$$EVM^2 = \frac{\mathbb{E}(|r'(t)|-|r(t)|)^2}{\mathbb{E}\left(|r(t)|^2\right)}. \tag{6}$$

We calculate the mean square error of $|r'(t)|$ where $t = nT_s$. Since we have $\mathbb{E}|r'(t)|^2 = \mathbb{E}|r(t)|^2$, using the Taylor expansion $\sqrt{1-x} = 1 - x/2 - x^2/8 + O(|x|^3)$ for small x, we get:

$$\begin{aligned} EVM^2 &= \frac{\mathbb{E}(|\mathrm{r}(\mathrm{t})|-|\mathrm{r}'(\mathrm{t})|)^2}{\mathbb{E}|r(t)|^2} = 2 - 2\frac{\mathbb{E}\left(\sqrt{|r'(t)|^2 |r(t)|^2}\right)}{\mathbb{E}|\mathrm{r}(\mathrm{t})|^2} \\ &\approx \frac{1}{4\mathbb{E}|r(t)|^2} \mathbb{E}\left(\frac{|r(t)|^2-|r'(t)|^2}{|r(t)|}\right)^2. \end{aligned} \tag{7}$$

By the definition of $r'(t)$ given in eq.(1), we obtain:

$$EVM^2 = \frac{1}{4\mathbb{E}|r(t)|^2} \int_{-\infty}^{\infty}\int_{-\infty}^{\infty}\int_{-\infty}^{\infty}\int_{-\infty}^{\infty} \mathbb{E}\left(X_{LO}(f_1)\overline{X_{LO}(f_2)}X_{LO}(f_3)\overline{X_{LO}(f_4)}\right) e^{2\pi j(f_1-f_2+f_3-f_4)t} \cdot e^{-jk(f_1^2-f_2^2+f_3^2-f_4^2)} \cdot \mathbb{E}\frac{\left(r(t-\frac{kf_1}{\pi})\overline{r(t-\frac{kf_2}{\pi})}-|r(t)|^2\right)\left(r(t-\frac{kf_3}{\pi})\overline{r(t-\frac{kf_4}{\pi})}-|r(t)|^2\right)}{|r(t)|^2} df_1 df_2 df_3 df_4. \tag{8}$$

Note that phase noise terms at different frequencies have zero correlation. To make $\mathbb{E}\left(X_{LO}(f_1)\overline{X_{LO}(f_2)}X_{LO}(f_3)\overline{X_{LO}(f_4)}\right)$ non-zero, (f_1, f_2, f_3, f_4) must pair up into two pairs with appropriate conjugation. There are two possibilities: $(f_1 = f_2, f_3 = f_4)$, and $(f_1 = f_4, f_2 = f_3)$, leading to the following decomposition:

$$\begin{aligned} EVM^2 &= \frac{1}{4\mathbb{E}|r(t)|^2} \int_{-\infty}^{\infty}\int_{-\infty}^{\infty} S(f_1)S(f_3)\mathbb{E}\left(\frac{1}{|r(t)|^2}|r(t-\frac{kf_1}{\pi})|^2|r(t-\frac{kf_3}{\pi})|^2-|\mathrm{r}(\mathrm{t})|^2\right) df_1 df_3 \\ &+ \frac{1}{4\mathbb{E}|r(t)|^2} \int_{-\infty}^{\infty}\int_{-\infty}^{\infty} S(f_1)S(f_3)\mathbb{E}\left(\frac{1}{|r(t)|^2}\left|r(t-\frac{kf_1}{\pi})\overline{r(t-\frac{kf_3}{\pi})}-|r(t)|^2\right|^2\right) df_1 df_3 \\ &= \frac{1}{4}(I_1+I_2), \end{aligned} \tag{9}$$

For the first term I_1, by doing mathematical calculation as shown in Appendix A, we obtain:

$$I_1 \approx a' \frac{k \cdot \Delta \nu}{T_s}, \tag{10}$$

Then we calculate $I_2 - I_1$ to obtain the second term I_2 as presented in Appendix B, direct calculation yields:

$$I_2 - I_1 \approx a\frac{k \cdot \Delta \nu}{T_s} + 2\int_{-\frac{T_s}{2k}}^{\frac{T_s}{2k}} \frac{k^2 f^2}{T_s^2} S(f) df \tag{11}$$

Putting eq.(10) and (11) together into eq.(9):

$$\begin{aligned} EVM^2 &= \frac{1}{4}(I_1+I_2) = \frac{1}{2}I_1 + \frac{1}{4}(I_2 - I_1) \\ &\approx \frac{a+2a'}{4}\frac{k \cdot \Delta \nu}{T_s} + \frac{1}{2}\int_{-\frac{T_s}{2k}}^{\frac{T_s}{2k}} \frac{k^2 f^2}{T_s^2} S(f) df \end{aligned} \tag{12}$$

For the second term $\int_{-\frac{T_s}{2k}}^{\frac{T_s}{2k}} \frac{k^2 f^2}{T_s^2} S(f) df$, it depends only on Δf_{pp} but not on f_t. This is the reason why the jitter tone mask in Fig.5(d) is flat above a corner frequency. Note that the following identity holds true for series associated to Bessel J functions:

$$\sum_{n=-\infty}^{\infty} n^2 J_n(\beta)^2 = \frac{\beta^2}{2}. \tag{13}$$

Since $\Delta f_{pp}, f_t \ll T_s / k$, we have:

$$\begin{aligned} &\int_{-\frac{T_s}{2k}}^{\frac{T_s}{2k}} \frac{k^2 f^2}{T_s^2} S(f) df \\ &\approx \int_{-T_s/2k}^{T_s/2k} \frac{k^2 f^2}{T_s^2}\left(\sum_{n=-\infty}^{\infty} w_n \cdot S_l(f-nf_t)\right) df \\ &= w_0 \int_{-\frac{T_s}{2k}}^{\frac{T_s}{2k}} \frac{k^2 f^2}{T_s^2} \frac{\Delta \nu}{\pi(\Delta \nu^2 + f^2)} df + \sum_{n\neq 0} w_n \int_{-\frac{T_s}{2k}}^{\frac{T_s}{2k}} \frac{k^2 f^2}{T_s^2} \frac{\Delta \nu}{\pi(\Delta \nu^2 + (\mathrm{f}-nf_t)^2)} df \\ &\approx w_0 \int_{-\frac{T_s}{2k}}^{\frac{T_s}{2k}} \frac{k^2 f^2}{T_s^2} \frac{\Delta \nu}{\pi(\Delta \nu^2 + f^2)} df + \sum_{n\neq 0} w_n \int_{-\frac{T_s}{2k}}^{\frac{T_s}{2k}} \frac{k^2}{T_s^2} \frac{(\mathrm{f}^2 + nf_t f + n^2 f_t^2)\Delta \nu}{\pi(\Delta \nu^2 + f^2)} df \\ &\approx \int_{-\frac{T_s}{2k}}^{\frac{T_s}{2k}} \frac{k^2 f^2}{T_s^2} \frac{\Delta \nu}{\pi(\Delta \nu^2 + f^2)} df + \frac{k^2}{T_s^2} \sum_{n=-\infty}^{\infty} w_n n^2 f_t^2 \\ &= a' \frac{k \cdot \Delta \nu}{T_s} + c\frac{k^2 \Delta f_{pp}{}^2}{T_s^2} \end{aligned} \tag{14}$$

Therefore, the EVM can be decomposed into two parts, representing the contribution from white noise and sinusoidal frequency jitter, respectively:

$$\begin{aligned} &EVM^2 = EVM_1{}^2 + \alpha \cdot EVM_2{}^2, \\ &EVM_1{}^2 \propto k \cdot \Delta \nu / T_s \propto L \cdot \Delta \nu / T_s, \\ &EVM_2{}^2 \propto k^2 \cdot \Delta f_{pp}{}^2 / T_s{}^2 \propto L^2 \cdot \Delta f_{pp}{}^2 / T_s{}^2. \end{aligned} \tag{15}$$

In essence, this means that the integral under Lorentzian distribution (in Eq.(5)) at carrier frequency leads to the term EVM_1^2, representing the contribution from white noise; while each frequency-shifted, weighted term in Eq.(5) contributes to the EVM_2^2 term, representing the effect of sinusoidal frequency jitter. The relative weight α are independent of the fiber length, baud rate, and laser linewidth, but may vary with different DSP algorithms. The exact value of α can be obtained through numerical analysis, as illustrated in Sec. IV B.

The theoretical analysis above illustrates the dependence of EVM on baud rate, fiber distance, laser linewidth, and the peak-to-peak interfering tone amplitude. The result is suitable for different constellations. It is worth noting that, for higher order QAM, the required EVM would be more stringent, in this case, the system tolerance to laser linewidth and frequency jitter tone amplitude would be reduced.

This article has been accepted for publication in a future issue of this journal, but has not been fully edited. Content may change prior to final publication. Citation information: DOI 10.1109/JLT.2019.2952725, Journal of Lightwave Technology

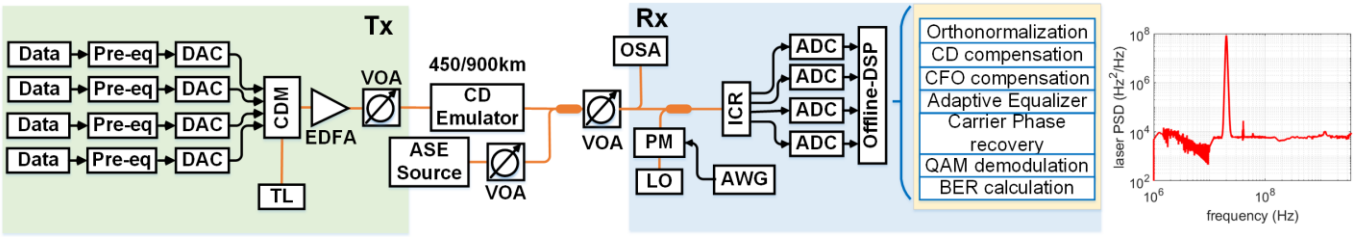

Fig 3. Experimental setup of the 64/32-Gbaud DP-16QAM coherent transmission. Pre-eq: Pre-equalization, TL: Tunable laser, CDM: coherent driver modulator, DAC: digital-to-analog convertor, EDFA: Erbium-doped fiber amplifier, OSA: optical spectrum analyzer, PM: phase modulator, ICR: Intradyne coherent receiver. Inset: Frequency noise PSD of the phase modulated LO with a 20 MHz tone and Δf_{pp} = 25.77 MHz.

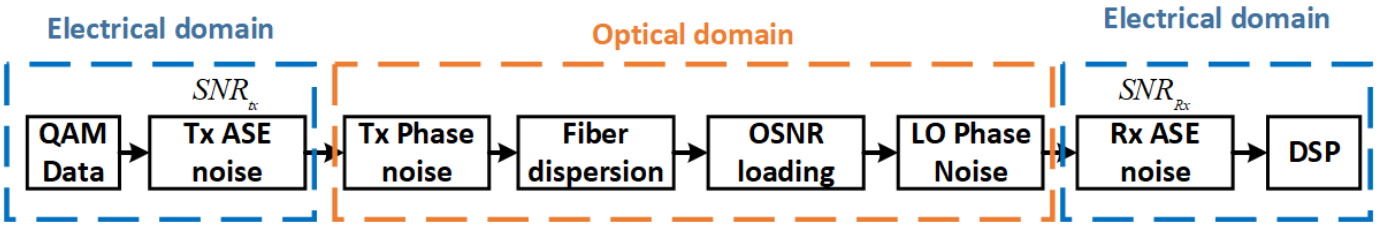

Fig 4. Simulation block diagram of the coherent systems.

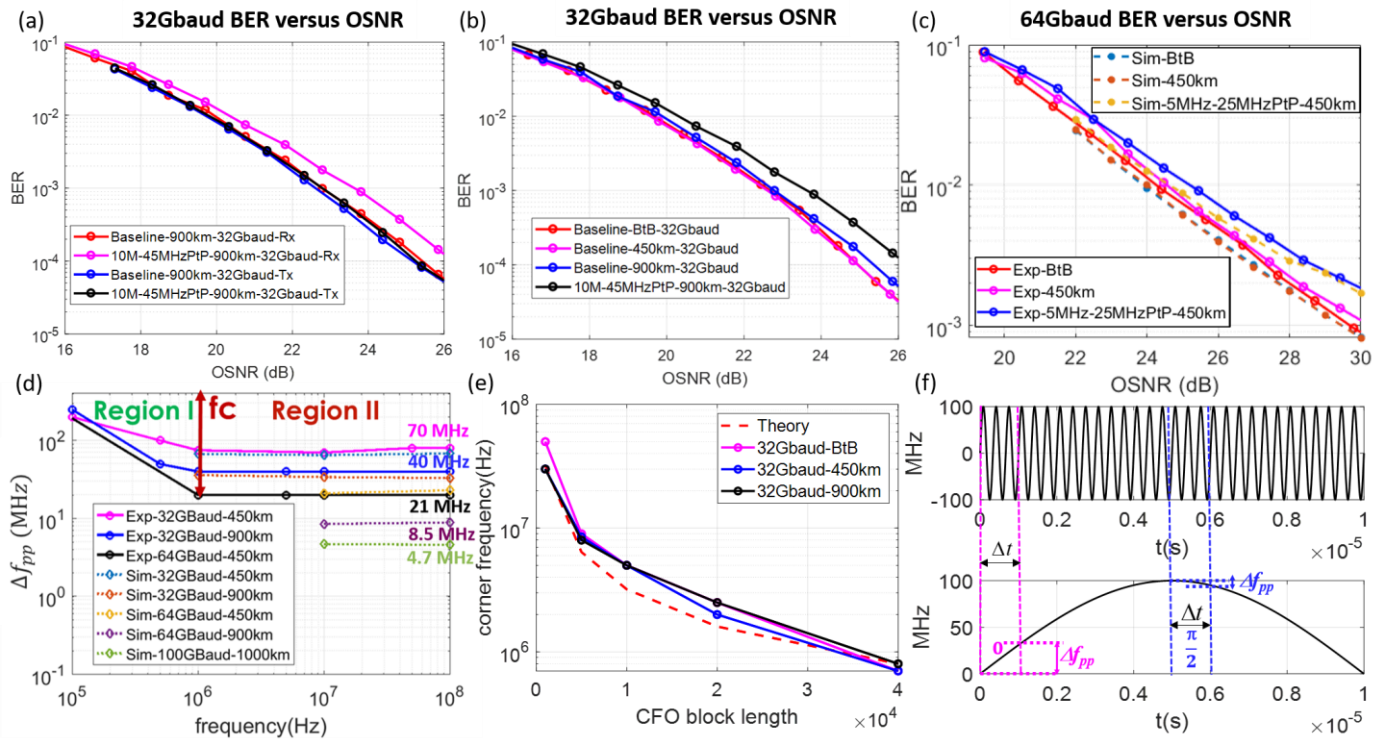

Fig 5. Experimental results with single jitter interference (rec. opt. power= -8dBm). (a) Benchmarks of BER versus OSNR between adding jitter interference at transmitter and receiver side in 32-Gbaud 900-km transmission with a 10-MHz tone and Δf_{pp} = 45 MHz. (b) BER versus OSNR for 32-Gbaud DP-16QAM BtB/450/900-km transmission with a 10-MHz sinusoidal tone and Δf_{pp} =45MHz causing 0.8dB OSNR penalty. (c) BER versus OSNR for 64-Gbaud DP-16QAM BtB/450-km transmission with a 5-MHz sinusoidal tone and Δf_{pp} =25 MHz causing 0.8dB OSNR penalty. (d) Single sinusoidal jitter tolerance versus sinusoidal frequency, at 0.5dB rOSNR penalty, for various baud rates and distances. (e) Corner frequency versus CFO block length in symbols for 32-Gbaud transmission. (f) Time domain expression of the effective frequency deviation Δf_{pp} as a function of the initial phase of the sinusoidal tone. (Upper diagram: Jitter tone with higher f_t; lower diagram: jitter tone with lower f_t .)

III. Experimental Setup and Simulation Procedure

A. Experimental Setup

Figure 3 shows the experimental setup of the DP-16-QAM coherent optical system to investigate the impact of the laser frequency jitter tone. Both the transmitter and LO external cavity lasers (ECLs) had a linewidth of 35 KHz and operating at a frequency around 193.5 THz. Four uncorrelated data sequences were applied with pre-equalizer with 11 taps and then were loaded to four 64 GSa/s digital to analog converters (DACs) operating at 1 Sa/symbol. The signal is then modulated by a coherent driver modulator (CDM), whose 3dB bandwidth was 40 GHz and V_π was 2V. A CD emulator with an 8-dB insertion loss was used to emulate a total CD of 450 or 900 km standard single-mode fiber (SSMF). Comparing to using SSMF spools and in-line EDFAs, the CD emulator completely

removes the concern of mixing fiber nonlinearity in the study. At the receiver side, a phase modulator and a low-speed arbitrary waveform generator (AWG) were used to modulate the LO with a sinusoidal tone by loading a sine wave to the AWG. As presented in the inset of Fig. 3, after PM, the laser frequency noise PSD exhibits a sharp peak at 20 MHz with a peak-to-peak amplitude (Δf_{pp}) equals 25.77 MHz (Note that 25.77MHz was obtained as follows: The peak of the frequency noise PSD in Fig.3 is 83e6 Hz^2/Hz, and the corresponding resolution bandwidth is 1e6 Hz, and we obtain the Δf_{pp} from $2\sqrt{2}\times\sqrt{83e6\times 1e6}=25.77MHz$. By changing the driving voltage of the PM and the period of the loading sine wave, we can sweep Δf_{pp} and frequency (f_t) of the sinusoidal tone in the experiment. After the intradyne coherent receiver (ICR), a 4-channel 80-GSa/s real-time scope captures the data at 1.25 Sa/symbol. In the offline-DSP, the data is resampled to 2 Sa/symbol, orthonormalized using Gram-Schmidt orthogonalization procedure, followed by CD and CFO compensation, polarization demultiplexing and equalization with 64 taps 4x2 butterfly adaptive equalizer, and blind-phase search carrier phase recovery (CPR).

B. Simulation

The simulation procedure is shown in Fig. 4. Firstly, we measured the signal EVM (based on average normalization) at the transmitter and receiver in a back-to-back setup to obtain EVM_{tx} and EVM_{total}, respectively, and convert them to electrical SNR_{tx} and SNR_{total}, respectively, through $EVM^2=\frac{1}{SNR}$ (which is valid for a high OSNR, required for baud rate ≥64Gbaud and modulation order ≥16QAM) [20]. The transmitter SNR_{tx} includes the booster EDFA's and DAC's ASE noise, as shown in Fig.4. The receiver SNR (SNR_{Rx}), which accounts for the ICR and ADC induced SNR degradation, can be obtained from $\frac{1}{SNR_{total}}=\frac{1}{SNR_{tx}}+\frac{1}{SNR_{Rx}}$. Secondly, the transmitter laser phase noise is based on a 35kHz linewidth, and the receiver LO phase noise is based on a 35kHz linewidth with jitter tone. Thirdly, the transmission link is modeled as $g(f)=\exp\left(-j\frac{\pi\cdot c\cdot L\cdot CD\cdot f^2}{(f_c-f)^2}\right)$ [21], where f_c is the carrier frequency, L is the fiber length, and CD is the fiber dispersion coefficient. CD is set as 17 ps/(nm×km) in simulation. Finally, ASE noise loading was applied to the received optical signal in order to vary the received OSNR.

In the simulation, we used a roll off factor of 0.2 for 64-Gbaud and 0.1 for 100-Gbaud systems, respectively, in order to match with the experimental signal spectrum. Note also that the same DSP was used for both the simulation and experiment.

IV. Experimental and Simulation Results

A. Jitter tone tolerance mask

As shown in Fig.5 (a), firstly, we compare the BER versus OSNR performance between loading frequency jitter tone at the transmitter laser and LO in a 32-Gbaud 900-km DP-16 QAM system. We set the bit error rate (BER) curve without sinusoidal interference as a baseline. We can observe that a 10-MHz tone with Δf_{pp} = 45 MHz at LO side induces 0.8-dB optical signal to noise ratio (OSNR) penalty at the BER of 1e-2. On the other hand, the curve of the same tone at the transmitter side overlaps with baseline and shows no penalty. This is because the transmitter laser phase noise has little impact on the system performance [4]. Therefore, in the following study, we will focus on the system performance effect due to a sinusoidal frequency jitter tone imposed on an LO only.

Figure 5 (b) and (c) illustrate the BER versus OSNR after adding a sinusoidal frequency jitter tone to an LO in 32- and 64-Gbaud transmission systems, respectively. In 32-Gbaud 900-km transmission, a 10-MHz sinusoidal jitter with a Δf_{pp}= 45 MHz introduces a 0.8-dB OSNR penalty at a BER of 1e-2. In Fig.5 (c), a 5-MHz sinusoidal frequency jitter tone with a peak-to-peak frequency deviation Δf_{pp}= 25 MHz causes 0.8-dB OSNR penalty at a BER of 1e-2. Therefore, a higher baud rate system would be more sensitive to a frequency jitter tone, and therefore a smaller Δf_{pp} is required. Also, the dashed lines are the simulation results, which match well with the experimental results. Therefore, the BER versus OSNR curves established our baseline for both experiment and simulation.

Figure 5 (d) presents the measured LO frequency jitter mask, which is defined as the allowable Δf_{pp} versus the jitter frequency f_t with a certain penalty threshold. We swept the frequency and Δf_{pp} of the sinusoidal tone to get a 0.5-dB rOSNR penalty at BER = 1e-2 in both the experiment and simulation. Note that above a certain corner frequency, the jitter mask is independent of the tone frequency (for a fixed EVM or BER, baud rate, and transmission distance), as predicted in Eq.(15). The resultant frequency jitter mask includes various baud rates and transmission distances so that a trend can be revealed, i.e., a tighter mask is required when the baud rate is higher or the transmission distance is longer. For example, in a 32-Gbaud DP-16QAM 450-km transmission system, the maximum allowable Δf_{pp} is 70 MHz while it is reduced to 40 MHz when the transmission distance is increased to 900-km. For a 64-Gbaud transmission, the maximum allowable Δf_{pp} is reduced from 21 MHz to 8.5 MHz when the distance is extended from 450-km to 900-km. The mask floor is further reduced to 4.7 MHz for a 100 Gbaud DP-16QAM signal over 1000 km. Based on the measured Δf_{pp} range of a few MHz in Fig.1, we can say that the impact of frequency jitter tone is of particular importance for 100 Gbaud/DP-16QAM and beyond, and for over 1000km. In Figure 5(d), it is worth noting that the frequency jitter mask is divided into two regions by a corner frequency f_c, which is inversely proportional to the block length (in time) of the CFO compensation. As shown in Fig.5 (e), the corner frequency is roughly proportional to $1/\left(Block\ Length\ of\ symbols\cdot T_s\right)$.The block length (in number of symbols × T_s) corresponds to the CFO estimator observation time. In CFO estimation, we usually utilize a sufficient long block size to get a more accurate CFO value. However, the longer the CFO block length, the longer the observation time of phase noise [15], which in turn causing a reduced corner frequency and a tighter jitter mask.

This article has been accepted for publication in a future issue of this journal, but has not been fully edited. Content may change prior to final publication. Citation information: DOI 10.1109/JLT.2019.2952725, Journal of Lightwave Technology

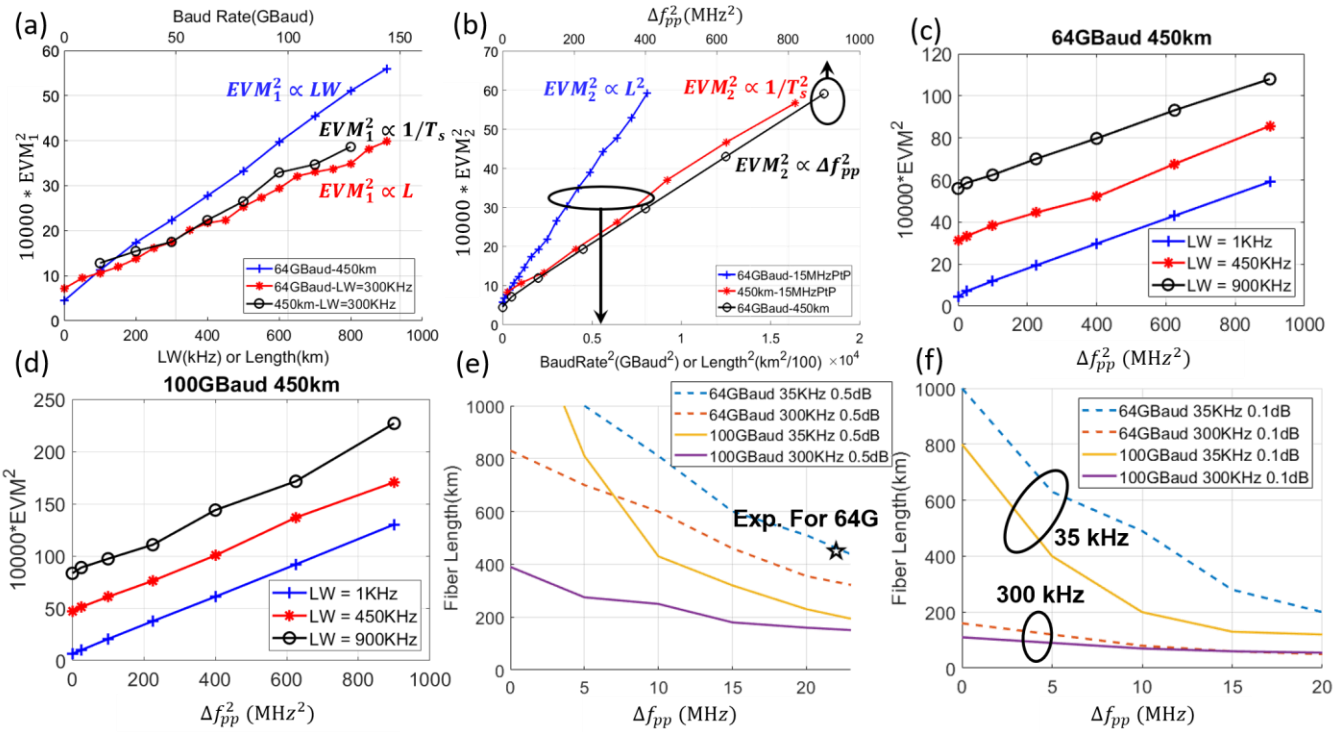

Fig 6. Simulation results (for 64Gbaud/DP-16QAM signals) with single jitter sinusoidal tone. (a) EVM_1^2 versus $\Delta\nu$, fiber length, and baud rate, with $EVM_2 = 0$ (Δf_{pp} = 0). (b) EVM_2^2 versus Δf_{pp}^2, (fiber length)^2, and (baud rate)^2, with a fixed small EVM_1 (laser linewidth =1 kHz). (c) EVM^2 versus single tone Δf_{pp}^2 with different laser linewidths at 64-Gbaud/DP-16QAM, 450-km transmission. (d) EVM^2 versus single tone Δf_{pp}^2 with different laser linewidths for 100-Gbaud/DP-16QAM, 450-km transmission. Fiber reach versus Δf_{pp} with 35 and 300 kHz intrinsic linewidth for (e) 0.5-dB penalty at BER = 1e-2 in 64/100-Gbaud DP-16QAM transmission, and (f) 0.1-dB penalty at BER = 1e-2 in 64/100-Gbaud DP-16QAM transmission.

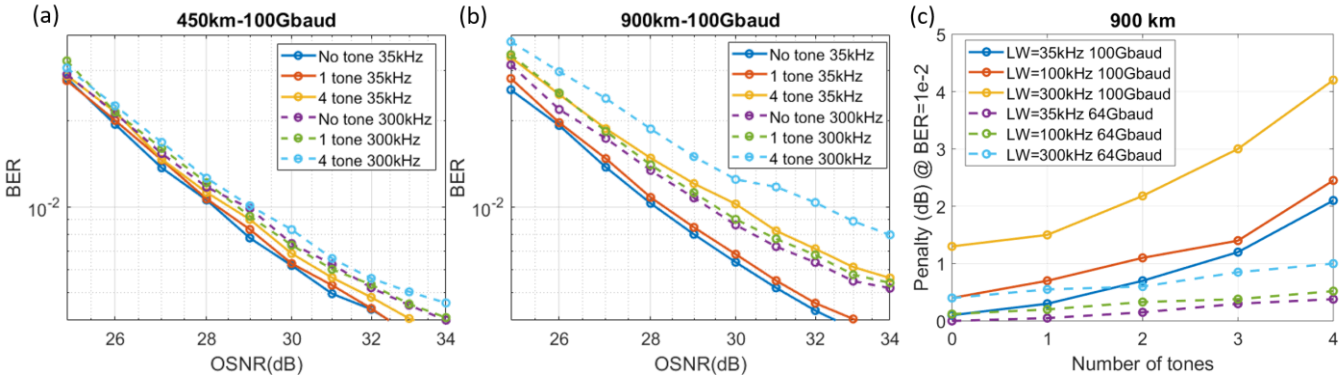

Fig.7. Simulation results of the impact of multiple tones (Δf_{pp} = 5 MHz) when the LO linewidth is either 35KHz or 300KHz. BER versus OSNR in 100-Gbaud DP-16QAM transmission with the impact of different linewidths and number of tones: (a) with 450-km fiber and (b) 900-km fiber. (c) Penalty at the BER of 1e-2 versus number of tones in in 64/100-Gbaud DP-16QAM 900-km transmission in cases of different linewidth.

The slow frequency drift in region I does not affect laser lineshape [7] and is handled by the CFO compensation section in a receiver DSP, while the faster frequency jitter in region II affects the laser lineshape and results in phase variance as well as EEPN. Fig.5(f) illustrates that the frequency deviation in region I is not only determined by Δf_{pp} but also related to initial phase when the jitter tone does not complete a period in the observation time [7, 22]. In our experiment, the observation time is around 1 μs. Take Fig.5(f) as an example, the observation time is about the time interval between the two dashed lines with the same color, which lasts for Δt. The higher frequency jitter (frequency > $1/\Delta t$)such as the upper curve can complete at least one period for the whole observation time while the lower frequency jitter (lower curve) may or may not complete a complete cycle depending on the initial phase. Therefore, during a fixed observation time, higher frequency interfering tones should induce the same Δf_{pp} independent of the initial phase. However, for lower frequency interfering tones, the induced effective Δf_{pp} could vary depending on the initial phase. For instance, as shown in the lower curve in Fig 5(f), the π initial phase induces larger Δf_{pp} than $\pi/2$ initial phase since it has a sharper slope. In Region I, i.e., the lower frequency region, we have swept the initial phase

of tones and chosen the worst case Δf_{pp} to ensure the tightest Δf_{pp} tolerance. As for Region II, the performance will not be determined by the initial phase and it is only dependent on Δf_{pp}. As shown in Fig. 5 (f), since Region II exhibits higher frequency, the jitter source can always complete several periods during the observation time. For back-to-back (BtB) transmission, the tolerance in region II is dominated by CPR capability. In addition, after CD emulator, the tolerance mask is much tighter with the increasing of baud rate and dispersion distances due to EEPN. EEPN cannot be mitigated by CPR and introduces timing error and amplitude distortions. Thus, the frequency jitter tolerance in region II is obviously much tighter than that of region I.

In the following analysis, we focus on the system impact of frequency jitter tones in Region II because that is where the worst performance occurs, and the performance is only dependent on Δf_{pp}.

B. *Verification of theoretical analysis*

Here we verify the validity of eq.(15) which gives the combined effect of laser linewidth and LO frequency jitter. Fig. 6(a) demonstrates the proportionality of the EVM_1^2 caused by the white frequency noise (through simulation) by setting EVM_2^2 to zero. Fig. 6(b) demonstrates the proportionality of the EVM_2^2 caused by the sinusoidal frequency jitter (through simulation) by setting EVM_1^2 to a small value with laser $\Delta\nu$ equals to 1kHz. Note all results are obtained for a 64Gbaud DP-16QAM system. In Fig.6(b), EVM_2^2 versus L^2 is obtained with the Δf_{pp} = 15 MHz, EVM_2^2 versus baud rate^2 is obtained with Δf_{pp} = 15 MHz and L = 450 km, and EVM_2^2 versus Δf_{pp}^2 is presented with 450-km transmission.

Figure 6(c) and (d) show the simulation results of EVM^2 versus Δf_{pp}^2 at a transmission distance of 450 km for three different laser linewidths of 1, 450, and 900 kHz for 64-Gbaud/DP-16QAM 450-km transmission and 100-Gbaud/DP-16QAM 450-km transmission, respectively. These result prove that EVM_1^2 (due to laser linewidth) and EVM_2^2 (due to LO frequency jitter) are additive since the three curves are parallel and show even gap between curves. In addition, We can observe in Figures 6(c) and 6(d) that for the same EVM^2, in case of 64-Gbaud/DP-16QAM transmission, a change in $\Delta\nu$ of 450 kHz is equivalent to a change in Δf_{pp}^2 of approximately $400\ \mathrm{MHz}^2$. For 100-Gbaud/DP-16QAM system, a change of 450 kHz in linewidth is the same as a change in Δf_{pp}^2 of approximately $300\ \mathrm{MHz}^2$. By plugging the value in the curves of either Fig.6(c) or Fig.6(d) into equation (15), we can obtain the numerical conclusion:

$$\begin{aligned} EVM^2 &= EVM_1^2 + 0.09 \cdot EVM_2^2, \\ EVM_1^2 &= 0.46 \cdot k \cdot \Delta\nu / T_s, \\ EVM_2^2 &= 0.46 \cdot k^2 \cdot \Delta f_{pp}^2 / T_s^2. \end{aligned} \tag{16}$$

The relative weighting between EVM_1^2 and EVM_2^2 is 0.09, and it is independent on the baud rate. Note that EVM_1^2 is consistent with the conclusion in [4], which showed that $EVM_1^2 \approx 0.5 \cdot k \cdot \Delta\nu / T_s$.

With EVM_1^2 and EVM_2^2 given in Eq.(16), we obtain Figures 6(e) and 6(f) , for an OSNR penalty of 0.5dB and 0.1dB at a BER=1e-2, respectively, the achievable fiber distance versus Δf_{pp} for 64 and 100 Gbaud DP-16QAM, and for two laser linewidths of 35 and 300KHz. Experimental results, shown by the star symbol, are also included, which match well with the simulation results. Several interesting facts can be observed from Fig.6(e) and (f): (i) The transmission distance decreases faster for the smaller Δf_{pp}, and less so for the larger Δf_{pp}, which implies the higher sensitivity of transmission distance to the smaller LO frequency jitter range. (ii) Judging from Fig.6(e), for the typical range of Δf_{pp} (as discussed in Sec.1) of 0.5MHz to several MHz the 35KHz linewidth laser exhibits much longer fiber reach than that of the 300KHz linewidth laser. For instance, Fig.6(e) shows that for 100Gbaud DP-16QAM transmission, with Δf_{pp} equals to 5 MHz, 35 kHz linewidth extends the 300KHz linewidth's reach from 250 km to 800 km. (iii) The higher the baud rate, the shorter the transmission distance, which implies when the transmission baud rate is increased beyond 100Gbaud, laser linewidth close to or even lower than 35KHz would be required.

C. *Simulation for Multiple Interfering Tones*

In practice, multiple frequency jitter tones could occur (as shown in Fig.1). Therefore, we performed simulations of multiple tones with random initial phases. All of the tones are set as the same Δf_{pp} of 5 MHz. Fig.7 (a) and (b) illustrate the BER performance in 450-km and 900-km 100-Gbaud DP 16QAM transmission under the impact of multiple tones. For 450-km and a single tone, 300-kHz linewidth exhibits ~0.6-dB penalty at the BER of 1e-2 compared with that of a 35 kHz linewidth, while the penalty from the additional 4 jitter tones are not significant (around 0.25 dB). When the distance is increased to 900 km, the penalty from the additional 4 tones becomes higher. With four tones (f_t at 1MHz, 3MHz, 6MHz, and 10MHz), the additional penalty from tones is 2 dB for 35kHz and 2.5 dB for 300kHz while for a single tone the penalty is small (0.15 dB). It indicates that the existence of multiple jitter tones would result in a tighter frequency jitter mask in Fig.5(d). Figure 7(c) presents the result of the OSNR penalty (relative to back-to-back case without any interfering tone) at a BER of 1e-2 with respect to the number of jitter tones. With the increasing of the number of jitter tones, the penalty also increases. It is worth noting that the increasing of penalty is not linear but a bit exponential for the case of 100Gbaud. Moreover, the combined effect of higher laser linewidth and jitter tones would introduce more penalty in high baud rate transmission.

V. CONCLUSION

Through theoretical, simulations, and experiments, we have found that, while EVM^2 due to EEPN is proportional to (baud rate × LO linewidth × transmission distance) when considering only the laser linewidth effect [4], it is proportional to (baud

This article has been accepted for publication in a future issue of this journal, but has not been fully edited. Content may change prior to final publication. Citation information: DOI 10.1109/JLT.2019.2952725, Journal of Lightwave Technology

rate× frequency jitter tone peak-to-peak frequency drift × transmission distance)^2 when considering the sinusoidal frequency jitter tone effect. The latter is an important factor to consider for a transmission system performance because the sinusoidal jitter tones often occurs in a pluggable transceiver or line-card due to unavoidable switching power supplies and other circuit noise. We found that the total EVM^2 is the weighted sum of the contributions from laser linewidth and frequency jitter tone. As a result, it is expected that a narrower laser linewidth would provide a higher margin for LO frequency jitter tolerance.

The fact that a system performance is sensitive to LO sinusoidal frequency jitter indicates the importance of setting up a jitter tolerance mask shown in Fig.5(d) to qualify tunable lasers. In practice, Eq. (15) can be utilized to qualify the jitter tone tolerance mask with a certain EVM requirement with various fiber distances, baud rates, and laser linewidths. Also, we can sweep the jitter tone tolerance in a numerical or experimental analysis by using a phase modulator at the LO, as shown in Fig. 3. The higher the baud rate, the longer the transmission distance, the higher the order of modulation, and the more jitter tones would cause a tighter jitter tolerance mask.

APPENDIX

A. *Derviation of* I_1

The following analysis calculates I_1. For $t = nT_s$, we have $r(t) = c_n$. Since the process is stationary, namely, the distributions of signal and the phase noise do not change with n, without loss of generality, we can assume $n = 0$. Plugging in the expression for r(t) and expanding the square of summation, we obtain:

$$\begin{aligned}\mathbb{E}\frac{|r(t-\frac{kf_1}{\pi})|^2|r(t-\frac{kf_3}{\pi})|^2}{|r(t)|^2} &= \mathbb{E}\left(\frac{1}{|c_0|^2}\mathbb{E}\left(\left(\sum_m |c_m|^2 s_m^2(f_1)\right)\left(\sum_m |c_m|^2 s_m^2(f_3)\right)|c_0\right)\right)\\ &+\mathbb{E}\left(\frac{1}{|c_0|^2}\mathbb{E}\left(\sum_{m_1\neq m_2}|c_{m_1}|^2|c_{m_2}|^2 s_{m_1}(f_1)s_{m_2}(f_1)s_{m_1}(f_3)s_{m_2}(f_3)|c_0\right)\right)\\ &= Z_1(f_1,f_3)+Z_2(f_1,f_3)\end{aligned} \tag{17}$$

where we denote $s_n(f) = \mathrm{sinc}(kf/T_s + n\pi)$.

By plugging Eq. (17) into the first term in Eq.(9) , we can decompose $\mathbb{E}\frac{|r(t-\frac{kf_1}{\pi})|^2|r(t-\frac{kf_3}{\pi})|^2}{|r(t)|^2}$ into two terms, and write I_1 as:

$$I_1 = \frac{1}{\mathbb{E}|r(t)|^2}\int_{-\infty}^{\infty}\int_{-\infty}^{\infty} S(f_1)S(f_3)\left(Z_1(f_1,f_3)+Z_2(f_1,f_3)-1\right)df_1df_3$$

For Z_1, by changing the order of integration, we have:

$$\begin{aligned}Z_1(f_1,f_3) &= \mathbb{E}\left(\frac{1}{|c_0|^2}\mathbb{E}\left(\left(\sum_m |c_m|^2 s_m^2(f_1)\right)\left(\sum_m |c_m|^2 s_m^2(f_3)\right)|c_0\right)\right)\\ &= \mathbb{E}|c_0|^2 s_0^2(f_1)s_0^2(f_3)+\mathbb{E}|c_m|^2\left(\sum_{m\neq 0}s_0^2(f_1)s_m^2(f_3)+s_0^2(f_3)s_m^2(f_1)\right)\\ &+\mathbb{E}\frac{1}{|c_0|^2}\left(\sum_{m\neq 0}|c_m|^2 s_m^2(f_1)\right)\left(\sum_{m\neq 0}|c_m|^2 s_m^2(f_3)\right)\end{aligned}$$

For Z_2, direct calculation yields:

$$\begin{aligned}Z_2(f_1,f_3) &= \mathbb{E}\left(\frac{1}{|c_0|^2}\mathbb{E}\left(\sum_{m_1\neq m_2}|c_{m_1}|^2|c_{m_2}|^2 s_{m_1}(f_1)s_{m_2}(f_1)s_{m_1}(f_3)s_{m_2}(f_3)|c_0\right)\right)\\ &= \mathbb{E}\frac{1}{|c_0|^2}\left(\mathbb{E}|c_0|^2\right)^2\left[\left(\sum_m s_m(f_1)s_m(f_3)\right)^2-\sum_m s_m^2(f_1)s_m^2(f_3)\right]\\ &= \mathbb{E}\left(|c_0|^2\right)\left[\left(\frac{\sin(k(f_1-f_3)/T_s)}{(k(f_1-f_3)/T_s)}\right)^2-\sum_m s_m^2(f_1)s_m^2(f_3)\right]\\ &\approx \mathbb{E}\left(|c_0|^2\right)\left[1-\frac{1}{3}\left(\frac{k(f_1-f_3)}{T_s}\right)^2-\sum_m s_m^2(f_1)s_m^2(f_3)\right]\end{aligned}$$

The expression of I_1 relies on taking integral of Z_1 and Z_2 under the power spectral density S(f), which involves integrals of squared sinc function. In the following we first analyze the behavior of sinc functions in this problem. For $x \ll 1$, we use the following Taylor expansion of sinc function to approximately evaluate I_1:

$$\mathrm{sinc}(x) = 1-\frac{1}{6}x^2+O(x^4),\quad \mathrm{sinc}(x-m\pi) = \frac{(-1)^m x}{m\pi}+O(x^3).$$

By making the decomposition $kf_i/T_s = q_i + x_i$, with integer q_i and $|x_i| < 1/2$, for $i = 1,2,3,4$. By the Taylor expansion approximation, we have:

$$s_m(f_i) = \begin{cases}\dfrac{(-1)^{q_i-m}}{(q_i-m)\pi}x_i+O(x_i^3), & q_i \neq m\\ 1-\dfrac{1}{6}x_i^2+O(x_i^4), & q_i = m\end{cases}$$

When applying the power spectral densities as kernels, decomposing kf_i/T_s into $q_i + x_i$ and plugging in the Taylor approximation, we obtain:

$$\begin{aligned}\int_{-\infty}^{\infty}s_m^2(f)S(f)df &\approx \left(\frac{k}{T_s}\right)^2\sum_{q\neq m}\int_{-\frac{T_s}{2k}}^{\frac{T_s}{2k}}\frac{f^2}{\pi^2(q-m)^2}S\left(f+\frac{T_s}{k}q\right)df\\ &+\int_{-\frac{T_s}{2k}}^{\frac{T_s}{2k}}\left(1-\frac{k^2}{3T_s^2}f^2\right)S\left(\frac{T_s}{k}m+f\right)df\end{aligned}$$

In the second term, we are using the approximation $(1-x)^2 \approx 1-2x$ for small x.

In our problem, we have $T_s/k \gg \Delta f_{pp}, \Delta\nu$ ($T_s/k \in [10^9, 10^{11}]$, $\Delta f_{pp} \in [10^5, 10^8]$, $\Delta\nu \sim 10^5$). As derived in Section II.A, the power spectral density is approximated by a mixture of Lorentzian distributions $S(f) \approx \sum_{n=-\infty}^{\infty} w_n \cdot S_l(f - nf_t)$, with each mixture component centered at scale Δf_{pp} and with width $\Delta\nu$. For $|f| \geq T_s/k$, we can use $S(f) \approx \Delta\upsilon/\pi f^2$, and the integral within $[-T_s/k, T_s/k]$ will be calculated later using the mixture of Lorentz distributions derived in Section II.A. If $m = 0$, we have:

$$\begin{aligned}&\int_{-\infty}^{\infty}s_0^2(f)S(f)df\\ &\approx \frac{T_s}{k}\sum_{q\neq 0}\frac{1}{\pi^2q^2}S\left(\frac{T_sq}{k}\right)+\int_{-\frac{T_s}{2k}}^{\frac{T_s}{2k}}\left(1-\frac{k^2}{3T_s^2}f^2\right)S(f)df\\ &\approx 1-\frac{1}{3}\int_{-\frac{T_s}{2k}}^{\frac{T_s}{2k}}(kf/T_s)^2S(f)df+a_1\frac{k\cdot\Delta\nu}{T_s}\end{aligned}$$

This article has been accepted for publication in a future issue of this journal, but has not been fully edited. Content may change prior to final publication. Citation information: DOI 10.1109/JLT.2019.2952725, Journal of Lightwave Technology

The value of universal constant a_1 is independent of all other parameters, which can be explicitly calculated, but the specific value is irrelevant to our discussion and is dependent on the DSP algorithm that employed at the receiver side.

For the case of $m \neq 0$, we have:

$$\begin{aligned}
&\int_{-\infty}^{\infty} s_m^2(f) S(f) df \\
&\approx \left(\frac{k}{T_s}\right)^2 \sum_{\substack{q \neq m \\ q \neq 0}} \int_{-\frac{T_s}{2k}}^{\frac{T_s}{2k}} \frac{f^2}{\pi^2 (q-m)^2} S\left(\frac{T_s q}{k}\right) df + S\left(\frac{T_s m}{k}\right) \int_{-\frac{T_s}{2k}}^{\frac{T_s}{2k}} \left(1 - \frac{k^2}{3T_s^2} f^2\right) df \\
&\quad + \frac{1}{\pi^2 m^2} \int_{-\frac{T_s}{2k}}^{\frac{T_s}{2k}} (kf / T_s)^2 S(f) df \\
&\approx \frac{1}{\pi^2 m^2} \int_{-\frac{T_s}{2k}}^{\frac{T_s}{2k}} (kf / T_s)^2 S(f) df + a_2 \frac{k \cdot \Delta\nu}{m^2 T_s}.
\end{aligned}$$

Similar to a_1, a_2 is a universal constant that does not change with other parameters.

Going back to I_1, we need the integral of $Z_1(f_1, f_3)$ under the kernel $S(f_1)S(f_3)$. By plugging in the approximate formulae for each term in the expression of $Z_1(f_1, f_3)$, we obtain:

$$\begin{aligned}
&\frac{1}{\mathbb{E}|c_0|^2} \int_{-\infty}^{\infty}\int_{-\infty}^{\infty} Z_1(f_1, f_3) S(f_1) S(f_3) df_1 df_3 \\
&\overset{(i)}{=} \left(\int_{-\infty}^{\infty} s_0^2(f_1) S(f_1) df_1\right)\left(\int_{-\infty}^{\infty} s_0^2(f_3) S(f_3) df_3\right) + 2\sum_{m \neq 0}\left(\int_{-\infty}^{\infty} s_m^2(f_3) S(f_3) df_3\right)\left(\int_{-\infty}^{\infty} s_0^2(f_1) S(f_1) df_1\right) \\
&\quad + \left(\sum_{m \neq 0}\int_{-\infty}^{\infty} s_m^2(f_1) S(f_1) df_1\right)\left(\sum_{m \neq 0}\int_{-\infty}^{\infty} s_m^2(f_3) S(f_3) df_3\right) \\
&\overset{(ii)}{\approx} \left(1 - \frac{1}{3}\int_{-\frac{T_s}{2k}}^{\frac{T_s}{2k}} (kf_1 / T_s)^2 S(f_1) df_1 + a_1 \frac{k \cdot \Delta\nu}{T_s}\right)^2 \\
&\quad + 2\left(\sum_{m \neq 0} \frac{1}{\pi^2 m^2} \int_{-\frac{T_s}{2k}}^{\frac{T_s}{2k}} (kf / T_s)^2 S(f) df + a_2 \frac{k \cdot \Delta\nu}{m^2 T_s}\right)\left(1 - \frac{1}{3}\int_{-\frac{T_s}{2k}}^{\frac{T_s}{2k}} (kf_1 / T_s)^2 S(f_1) df_1 + a_1 \frac{k \cdot \Delta\nu}{T_s}\right) \\
&\quad + \left(\sum_{m \neq 0} \frac{1}{\pi^2 m^2} \int_{-\frac{T_s}{2k}}^{\frac{T_s}{2k}} (kf / T_s)^2 S(f) df + a_2 \frac{k \cdot \Delta\nu}{m^2 T_s}\right)^2 \\
&\overset{(iii)}{\approx} 1 - \frac{2}{3}\int_{-\frac{T_s}{2k}}^{\frac{T_s}{2k}} (kf_1 / T_s)^2 S(f_1) df_1 + a_1 \frac{k \cdot \Delta\nu}{T_s} + \left(\sum_{m \neq 0} \frac{2}{\pi^2 m^2}\right) \int_{-\frac{T_s}{2k}}^{\frac{T_s}{2k}} (kf / T_s)^2 S(f) df + a_2 \sum_{m \neq 0} \frac{k \cdot \Delta\nu}{m^2 T_s} \\
&\overset{(iv)}{=} 1 + \left(a_1 + \frac{\pi^2}{3} a_2\right) \frac{k \cdot \Delta\nu}{T_s}.
\end{aligned}$$

The above calculation involves four steps. Step (i) is by exchanging the order of summation and differentiation; step (ii) is by plugging in the approximate formulae for the squared integral of sinc functions; step (iii) is discarding high-order terms when the integrals are less than 1, and step (iv) is using the identity $\sum_{n \geq 1} n^{-2} = \frac{\pi^2}{6}$.

In the above calculation, we omit all the high order terms. The last squared term in the expression is negligible because it is of the same order of square of other terms.

For $Z_2(f_1, f_3)$, we have:

$$\begin{aligned}
&\int_{-\infty}^{\infty}\int_{-\infty}^{\infty} Z_2(f_1, f_3) S(f_1) S(f_3) df_1 df_3 \\
&\approx \left(\mathbb{E}|c_0|^2\right) \cdot \int_{-\infty}^{\infty}\int_{-\infty}^{\infty} \left[1 - \frac{1}{6}\left(\frac{k(f_1 - f_3)}{T_s}\right)^2 - \sum_m s_m^2(f_1) s_m^2(f_3)\right] S(f_1) S(f_3) df_1 df_3 \\
&\approx \left(\mathbb{E}|c_0|^2\right) \cdot \left(1 - \sum_m \left(\int_{-\infty}^{\infty} s_m^2(f) S(f) df\right)^2\right) \\
&\approx a^2 \left(\mathbb{E}|c_0|^2\right) \left(\frac{k \cdot \Delta\nu}{T_s}\right)^2
\end{aligned}$$

Since $k \cdot \Delta\nu / T_s \ll 1$, the integral of Z_2 is much smaller than $k \cdot \Delta\nu / T_s$, which is the scale of the integral of Z_1. Therefore, the contribution by Z_2 in the final expression of I_1 is negligible, and we obtain:

$$I_1 \approx a' \frac{k \cdot \Delta\nu}{T_s},$$

for some constant $a' > 0$.

B. Derivation of $I_2 - I_1$

Now we turn to the term I_2. Note that:

$$I_2 - I_1 = \frac{1}{4\mathbb{E}|c_0|^2} \iint_{\mathbb{R}^2} S(f_1) S(f_3) \mathbb{E}\left|r(t - \frac{kf_1}{\pi}) - r(t - \frac{kf_3}{\pi})\right|^2 df_1 df_3$$

Note that for $f_1, f_3 \ll T_s / k$, we have:

$$\begin{aligned}
&\mathbb{E}\left|r(t - \frac{kf_1}{\pi}) - r(t - \frac{kf_3}{\pi})\right|^2 = \mathbb{E}\left(|c_0|^2\right) \sum_m \left(s_m(f_1) - s_m(f_3)\right)^2 \\
&= 2\mathbb{E}\left(|c_0|^2\right)\left(1 - \frac{\sin\left(k(f_1 - f_3)/T_s\right)}{k(f_1 - f_3)/T_s}\right) \approx \frac{2}{3}\mathbb{E}\left(|c_0|^2\right)\left(\frac{k(f_1 - f_3)}{T_s}\right)^2.
\end{aligned}$$

And as in the estimate for I_1, the integral outside the region $[-T_s/2k, T_s/2k] \times [-T_s/2k, T_s/2k]$ is approximately a constant multiple of $k \cdot \Delta\nu / T_s$. Therefore, we have:

$$\begin{aligned}
I_2 - I_1 &\approx a \frac{k \cdot \Delta\nu}{T_s} + \int_{-\frac{T_s}{2k}}^{\frac{T_s}{2k}}\int_{-\frac{T_s}{2k}}^{\frac{T_s}{2k}} (k(f_1 - f_3)/T_s)^2 S(f_1) S(f_3) df_1 df_3 \\
&= a \frac{k \cdot \Delta\nu}{T_s} + \int_{-\frac{T_s}{2k}}^{\frac{T_s}{2k}}\int_{-\frac{T_s}{2k}}^{\frac{T_s}{2k}} \frac{k^2}{T_s^2} (f_1^2 + f_3^2 - 2 f_1 f_3) S(f_1) S(f_3) df_1 df_3 \\
&\approx a \frac{k \cdot \Delta\nu}{T_s} + 2\int_{-\frac{T_s}{2k}}^{\frac{T_s}{2k}} \frac{k^2 f^2}{T_s^2} S(f) df
\end{aligned}$$

The cross term integrates to zero because the power spectral density is a symmetric function.

REFERENCES

[1] G. Liu, K. Zhang, R. Zhang, R. Proietti, H. Lu, and S. J. Ben Yoo, "Demonstration of a carrier frequency offset estimator for 16-/32-QAM coherent receivers: a hardware perspective," *Optics Express*, vol. 26, pp. 4853-4862, 2018.

[2] G. Li, "Recent advances in coherent optical communication," *Advances in Optics and Photonics*, vol. 1, pp. 279-307, 2009.

[3] J. Buus and E. J. Murphy, "Tunable Lasers in Optical Networks," *Journal of Lightwave Technology*, vol. 24, p. 5, 2006.

[4] A. Kakkar, J. R. Navarro, R. Schatz, H. Louchet, X. Pang, O. Ozolins, *et al.*, "Comprehensive Study of Equalization-Enhanced Phase Noise in Coherent Optical Systems," *Journal of Lightwave Technology*, vol. 33, pp. 4834-4841, 2015.

[5] M. Iglesias Olmedo, X. Pang, R. Schatz, O. Ozolins, H. Louchet, D. Zibar, *et al.*, "Effective Linewidth of Semiconductor Lasers for Coherent Optical Data Links," *Photonics*, vol. 3, p. 39, 2016.

[6] W. Shieh and K.-P. Ho, "Equalization-enhanced phase noise for coherent-detection systems using electronic digital signal processing," *Optics Express*, vol. 16, pp. 15718-15727, 2008.

[7] A. Kakkar, J. Rodrigo Navarro, R. Schatz, X. Pang, O. Ozolins, A. Udalcovs, *et al.*, "Laser Frequency Noise in Coherent Optical Systems: Spectral Regimes and Impairments," *Scientific Reports*, vol. 7, p. 844, 2017.

[8] I. Fatadin and S. J. Savory, "Impact of phase to amplitude noise conversion in coherent optical systems with digital dispersion compensation," *Optics Express*, vol. 18, pp. 16273-16278, 2010.

[9] M. Al-Qadi, G. Vedala, and R. Hui, "Phase Noise of Diode Laser Frequency Comb and its Impact in Coherent Communication

Systems," in *Conference on Lasers and Electro-Optics*, San Jose, California, 2018, p. JTu2A.35.

[10] J. P. Wilde, G. W. Yoffe, and J. M. Kahn, "Frequency Noise Characterization of a Widely Tunable Narrow-Linewidth DFB Laser Array Source," in *Optical Fiber Communication Conference and National Fiber Optic Engineers Conference*, San Diego, California, 2009, p. JWA33.

[11] J. E. Simsarian, J. Gripp, S. Chandrasekhar, and P. Mitchell, "Fast-Tuning Coherent Burst-Mode Receiver for Metropolitan Networks," *IEEE Photonics Technology Letters*, vol. 26, pp. 813-816, 2014.

[12] L. D. Turner, K. P. Weber, C. J. Hawthorn, and R. E. Scholten, "Frequency noise characterisation of narrow linewidth diode lasers," *Optics Communications*, vol. 201, pp. 391-397, 2002.

[13] R. Zhang, W. Jiang, Jr., K. Kuzmin, R. Juluri, G.-K. Chang, and W. I. Way, "Laser Frequency Jitter Tolerance and Linewidth Requirement for > 64Gbaud DP-16QAM coherent systems," in *Optical Fiber Communication Conference (OFC) 2019*, San Diego, California, 2019, p. M4I.2.

[14] F. Cruz, R. Cavasso-Filho, A. Siqueira, D. Manoel, E. Telles, A. Scalabrin, *et al.*, "Laser Noise Measurements and Observation of Amplitude Squeezing in an Extended Cavity Diode Laser," *Revista de Féisica Aplicada e Instrumentaçc ao*, vol. 14, 1999.

[15] K. Kikuchi, "Characterization of semiconductor-laser phase noise and estimation of bit-error rate performance with low-speed offline digital coherent receivers," *Optics Express*, vol. 20, pp. 5291-5302, 2012.

[16] X. Chen, A. Al Amin, and W. Shieh, "Characterization and Monitoring of Laser Linewidths in Coherent Optical OFDM Systems," in *Optical Fiber Communication Conference/National Fiber Optic Engineers Conference 2011*, Los Angeles, California, 2011, p. OWN4.

[17] A. Demir, A. Mehrotra, J. Roychowdhury, and J. Roychowdhury, "Phase noise in oscillators: a unifying theory and numerical methods for characterisation," presented at the Proceedings of the 35th annual Design Automation Conference, San Francisco, California, USA, 1998.

[18] T. T. S. C. Sekhar, *Communication Theory*: Tata McGraw-Hill Education, 2005.

[19] A. P. T. Lau, T. S. R. Shen, W. Shieh, and K.-P. Ho, "Equalization-enhanced phase noise for 100Gb/s transmission and beyond with coherent detection," *Optics Express*, vol. 18, pp. 17239-17251, 2010.

[20] R. A. Shafik, M. S. Rahman, and A. R. Islam, "On the Extended Relationships Among EVM, BER and SNR as Performance Metrics," in *2006 International Conference on Electrical and Computer Engineering*, 2006, pp. 408-411.

[21] R. Kudo, T. Kobayashi, K. Ishihara, Y. Takatori, A. Sano, and Y. Miyamoto, "Coherent Optical Single Carrier Transmission Using Overlap Frequency Domain Equalization for Long-Haul Optical Systems," *Journal of Lightwave Technology*, vol. 27, pp. 3721-3728, 2009.

[22] W. Ng, A. T. Nguyen, S. Ayotte, C. Park, and L. A. Rusch, "Impact of Sinusoidal Tones on Parallel Decision-Directed Phase Recovery for 64-QAM," *IEEE Photonics Technology Letters*, vol. 26, pp. 486-489, 2014.